Morphological Diagram for Metal/Polymer Bilayer Wrinkling: Influence of Thermomechanical Properties of Polymer Layer

ARTICLE *in* MACROMOLECULES · APRIL 2005

Impact Factor: 5.8 · DOI: 10.1021/ma048452+

2 AUTHORS, INCLUDING:

Pil J. Yoo
Sungkyunkwan University (SKKU)
86 PUBLICATIONS **3,057** CITATIONS

SEE PROFILE

Morphological Diagram for Metal/Polymer Bilayer Wrinkling: Influence of Thermomechanical Properties of Polymer Layer

Pil J. Yoo and Hong H. Lee*

School of Chemical Engineering, Seoul National University, Seoul, 151-744, Korea

Received July 28, 2004; Revised Manuscript Received January 23, 2005

ABSTRACT: Three types of wrinkling are found to occur in the wrinkling of a bilayer of metal and polymer on a substrate. Each type has its own unique characteristics in terms of the wrinkle growth and strain behavior. While the characteristics can be grouped into three types, five distinct wrinkling regimes exist in terms of morphological change: evolutionary, constrained evolutionary, instantaneous, unconstrained, and spinodal wrinkling. The final morphologies for these wrinkling regimes are as follows: a labyrinth structure for the evolutionary wrinkling, an island structure for the constrained evolutionary and instantaneous wrinkling, a flat surface for the unconstrained wrinkling, and a mountainous structure for the spinodal wrinkling. A morphological diagram for these regimes and types can be constructed in terms of temperature and thickness of the polymer film with the molecular weight as a parameter. The characteristics and morphology are governed by the thermomechanical properties of the polymer as affected by temperature with the constraints stemming from strain saturation of the metal and pinning of the thin bilayer.

Introduction

Wrinkle formation in layered systems is a ubiquitous phenomenon and is often encountered in modern science and technology.[1−3] The wrinkles are believed to form spontaneously by the abrupt compressive stress, which is generated when the stress exceeds the critical compressive stress of the system that arises from a mismatch of thermal expansion coefficient between the substrate and the capping layer. The wrinkling phenomena have been treated as defects and degradations in layered structures because of their irregularity and uncontrollability.[4,5] Recently, however, patterning processes using elastic buckling have been presented, in which a prepatterned substrate[6−8] or an external confinement by a patterned mold[9] is utilized. As a result, one can easily obtain well-ordered sinusoidal wrinkles that can be useful for optical applications. Furthermore, the wrinkles can be modulated through wave interactions and tuned to various shapes[10,11] that can hardly be accessible by other patterning methods.

On the other hand, wrinkling on a viscous film has been studied extensively due to its importance in semiconductor industry and thin film processing.[12−14] In such a process, a technique called "compliant substrate" is used to relieve the accumulated compressive stress in the film processing by bonding an underlying substrate and an upper layer with a low viscosity glass. In the annealing process, the low viscosity glass melts and can flow, leading to slow buckling (wrinkling) of the film.

If the underlying layer is a viscoelastic material such as an amorphous polymer, however, the dynamics of wrinkling is much more complicated than in purely elastic or viscous wrinkling. In the bilayer system being considered, a thin polymer layer is capped with a thin metal layer. The polymer layer is strongly bonded to both the underlying substrate and upper metal layer. When the temperature is raised above the glass transition temperature of the polymer (T_g), the polymer layer relaxes and changes from an elastic glassy state to an elastically behaving rubbery state. If the temperature is raised further, the polymer layer finally turns into a viscously behaving fluidic state.[15] During this process, the thermal expansion coefficient of the polymer increases dramatically, by an order of magnitude ($60-80 \times 10^{-6}$ below T_g, $500-600 \times 10^{-6}$ above T_g),[16] and this large change in the coefficient brings about instability, which leads to the wrinkling. The relaxation behavior of the polymer is reflected in the wrinkle morphology. In our previous studies, we identified two regimes of wrinkling.[17,18] When the polymer behaves like an elastic rubber in moderate temperature range, which is slightly higher than the T_g of the polymer, elastic behavior dominates the system and the elastic wrinkling, which is characterized by the constancy of the wrinkle wavelength, can be described by a free energy approach.[17] When the polymer behaves like a viscous fluid in much higher temperature range, however, viscous behavior dominates and the wrinkling, which is characterized by growing wavelength, can be described by a kinetic approach.[18]

While temperature is a key variable, there are many other variables that can affect the wrinkling such as polymer film thickness, heating condition and time, molecular weight of the polymer, cross-linking level of the polymer, etc. All these variables, we find as described later, collectively affect the viscoelastic state of the polymer and the relaxation condition of the stress. These states and conditions are the ones that determine the wrinkling behavior. In this article, the finding is utilized in identifying five wrinkling regimes including the two found earlier, and these regimes are grouped into three types according to the common characteristics of the wrinkling behavior. A morphological phase diagram is given for these wrinkling regimes and types. Some of the earlier findings[17,18] are included for a coherent picture of the wrinkling.

* Corresponding author. E-mail: honghlee@snu.ac.kr. Telephone: 82-2-880-7403. Fax: 82-2-878-5043.

10.1021/ma048452+ CCC: $30.25
Published on Web 03/01/2005

Experimental Section

Preparation of Metal/Polymer Bilayer. A cleaned silicon (100) wafer was used as a substrate for the bilayer wrinkling. The substrate was cleaned by ultrasonic treatment in trichloroethylene and methanol for 5 min each and dried in nitrogen. Native oxide was not removed from the surface and thus would exist on the surface. For the polymer, polystyrene (PS), which is a typical amorphous linear polymer, was used because of its well-known physical properties. Two types of PS differing in molecular weight were used to investigate the influence of elastic or viscous behavior on the wrinkling. One is a high molecular weight PS for the rubbery elastic state (M_n = 1,340,000, M_w/M_n = 1.05, $T_g \approx$ 105 °C, Polymer Source Inc.) and the other is a low molecular weight PS for the fluidic viscous state (M_n = 8500, M_w/M_n = 1.06, $T_g \approx$ 80 °C, Polymer Source Inc.) Typically, a toluene solution of PS was spin-coated to a thickness ranging from 26 to 800 nm onto a silicon substrate by varying the solution concentration or the spin-coating speed. The samples were annealed at 60 °C for 12 h to remove the residual solvent and to relieve the stress due to the spin-coating. For the metal, we used aluminum as the capping layer due to its high ductility and good adhesion property with the underlying polymer layer. The aluminum was deposited onto the polymer surface, ranging in thickness from 30 to 80 nm, by thermal evaporation. The thermal deposition was carried out at a high deposition rate so as to minimize the thermal stress that could be generated due to the heating of the sample during the deposition process.

Surface Wrinkling and Characterization. To induce the wrinkling by thermal stress, the bilayer samples were heated to a temperature that is well above the T_g of PS (different depending on the molecular weight of PS). Annealing time was also varied from 12 h to 8 days depending on the morphological changes. The resulting metal surface structures were examined by atomic force microscopy (AFM, Digital Instruments, Dimension 3100 and Nanoscope IIIa) in the contact and tapping modes. Cross-sectional analysis by scanning electron microscopy (SEM) was also carried out to check the presence of any blisters that might have been generated by delamination. No blisters were found under the experimental conditions, and the underlying polymer layer conformed to the topography of the capping metal layer.

Theory: Energetic and Kinetic Descriptions of Wrinkling

Critical Stress for Wrinkling. During the heating process for wrinkling, a small amount of thermal stress is generated and accumulates in the bilayer. When the temperature is raised above the T_g of the polymer, the polymer loses its mechanical rigidity and its state changes to soft rubbery state, which results in a dramatic change in the thermal expansion coefficient. This change produces an abrupt, large amount of thermal stress that leads to the wrinkling. An incubation period exists for the wrinkling, duration of which depends on the bilayer thickness and the annealing temperature,[17,18] because the wrinkling is initiated when the accumulated stress exceeds the critical compressive stress for the wrinkling.

According to Allen,[19] the critical stress, δ_{cr}, for one-sided rigid substrate buckling is given as follows:[19]

$$\delta_{cr} = \frac{E_f}{12}\left(\frac{t_m}{t_p}\right)^2\theta^2 + E_p\left(\frac{t_p}{t_m}\right)f(\theta) \quad (1)$$

$$f(\theta) = \frac{2}{\theta}\frac{(3-\nu_p)\sinh\theta\cosh\theta + (1+\nu_p)\theta}{(1+\nu_p)(3-\nu_p)^2\sinh^2\theta - (1+\nu_p)^3\theta^2}, \ \theta \equiv \frac{2\pi t_p}{\lambda} \quad (2)$$

where t is the thickness, E is Young's modulus, the subscripts m and p are for the metal and the polymer, respectively, ν_p is the Poisson ratio of the polymer, and λ is the wavelength of the wrinkling wave. When the compressive stress of the bilayer exceeds the critical value, wrinkling takes place on the bilayer surface as an isotropic sinusoidal wave. As given in eqs 1 and 2, δ_{cr} is dependent on the thickness of the underlying polymer layer, t_p.

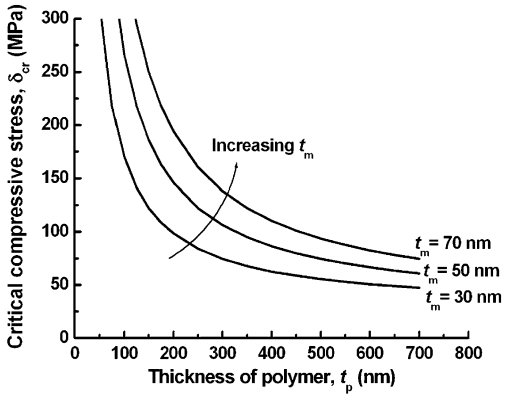

Figure 1. Dependency of the critical compressive stress on the thickness of polymer layer and that of the capping metal layer. Typical parameter values were used for the figure: E_m = 70 GPa, E_p = 1.8 MPa, μ_p = 0.33, and values of λ obtained from eq 8.

To show this dependence on t_p, we plotted the critical compressive stress against the polymer layer thickness in Figure 1. As shown in the figure, the critical stress increases gradually with decreasing polymer thickness up to 200 nm thickness. For the thickness smaller than about 200 nm, however, the critical stress increases rapidly with decreasing t_p because the wrinkling of the capping metal layer is highly suppressed due to the thickness restriction. To induce the wrinkling in this very thin metal/polymer bilayer, therefore, a heating temperature much higher than T_g is needed to increase the thermal stress. On the other hand, in this higher temperature range, polymer cannot maintain its elastic property any more, and consequently, it tends to behave like a viscous liquid.[15] Hence, the wrinkling process cannot be explained by the conventional energetic approach but by a kinetic approach. The thermomechanical behavior of the underlying polymer layer as affected by wrinkling conditions, therefore, would form a basis for describing the wrinkling behavior of the metal/polymer bilayer system. In what follows, two approaches, energetic and kinetic, are taken for the elastic-like and viscous-like polymer layer to provide a theoretical background for the wrinkling regimes and types.

Energetic Approach for Elastic-Like Polymer Layer. If the underlying polymer layer behaves like an elastic medium, the system can be explained by a static approach that is based on a free energy analysis. The underlying mechanism has been generally understood as a stress-driven instability, which is similar to the buckling of an elastic column under compression.[19−21] In the wrinkling process, the polymer and the metal maintain the bonding with each other and deform conformably in forming a wrinkled structure. As discussed earlier, there exists a critical compressive stress for wrinkling, beyond which the film deforms into wavy wrinkles with a certain characteristic wavelength. For an analysis of the wrinkle formation, a set of nonlinear partial differential equations, known as Föppl−von Kar-

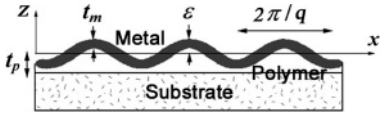

Figure 2. Schematic geometry of the bilayer of metal and polymer on a substrate.

man equations,[22−23] can be solved. The equations have a vertical displacement term and a shear stress term that are coupled, which makes them impossible to solve analytically except in some one-dimensional cases. To get a solution for other cases, therefore, one is forced to a numerical computation.

The bilayer system being considered is a polymer layer capped with a thin metal layer. When the system is heated slightly above the glass transition temperature of the polymer, the polymer gets softened and deforms conformably with the capping metal layer during the wrinkling. Unlike buckling or delamination of a single plate, therefore, the deformation of the underlying polymer layer plays an important role in the wrinkling. In this case, the system can simply be described by two competing energy terms. One is the contribution from the bending of the metal layer in forming the wrinkles and the other from the deformation of the polymer layer to conform to the wrinkled metal layer.[17]

For a sinusoidal deformation in one direction, a low amplitude ($t_m q \ll 1$) wave profile $w(x) = \epsilon \sin(qx)$ can be assumed, where ϵ is the amplitude of the wave and q is the wavenumber. Referring to Figure 2 for the bilayer system, the free energy per unit area (per oscillation mode) to bend the metal film can be written as[24]

$$F_{Bending} = \frac{E_m {t_m}^3}{48(1-{\nu_m}^2)}\epsilon^2 q^4 \tag{3}$$

where ν_m is the Poisson ratio of the metal layer. For the free energy of deformation of the elastic polymer film, we turn to the free energy expression of a distorted elastic film, which is often taken as a polymer brush model.[25,26] This model is well matched with our bilayer system, because the polymer layer is bound with and confined between the substrate and the capping metal layer such that the elastic behavior is maximized.[27,28] Although the upper aluminum layer is different from the free surface in the polymer brush model, the strong binding between the polymer and aluminum makes it possible to fully transfer the local stretching of polymer to the buckling wave, which would not leave any tangential stress at the top polymer layer just as at the free surface in the polymer. Therefore, the same boundary condition can be applied to this metal/polymer layered system. Furthermore, a sinusoidal surface wrinkle makes the polymer deform into a perfectly wavy shape, hence the ideal sinusoidal stretching model in the elastic analysis can be applied to the deformation of the polymer layer.

To get an expression for the free energy of the elastic film, we adopt the conventional notation of Landau and Lifshitz[22] and the analysis by Frederickson et al.[25] Hooke's law provides the relationship between the stress and the strain. To express the stress as a function of x and z (refer to Figure 2), the displacement fields under sinusoidal perturbation are obtained as in the literature,[22,25] which gives $u_x = \epsilon\Psi_1(z)\sin(qx)$ and $u_z = \epsilon\Psi_2(z)\cos(qx)$, and $\Psi_i(z)$ $(i = 1, 2)$ are given by $\Psi_1(z) = C_1[\sinh(qz) + qz\cosh(qz)] + C_2 qz\sinh(qz)$ and $\Psi_2(z) = C_2[\sinh(qz) - qx_2\cosh(qz)] - C_1 qx_2\sinh(qz)$. When the incompressibility condition is applied, the complicated coefficients C_i can be simplified with a dimensionless variable, qh_0, to

$$C_1(qh_o) = \frac{qh_0\cosh(qh_0)}{qh_0 - \cosh(qh_0)\sinh(qh_0)},$$
$$C_2(qh_0) = -\frac{\cosh(qh_0) + qh_0\sinh(qh_0)}{qh_0 - \cosh(qh_0)\sinh(qh_0)} \tag{4}$$

where h_0 is the thickness of the initial film. The excess free energy per unit area of the deformed film, F_{deform}, can be written in the form

$$F_{\text{deform}} = \frac{q}{2\pi}\int_0^{2\pi/q} dx \int_0^{h_0} \frac{E_p}{3}({u_{11}}^2 + {u_{22}}^2 + 2{u_{12}}^2)dz \tag{5}$$

where the strain field u_{ij} are obtained from the appropriate derivatives of the strain terms. The integrals in eq 5 can be carried out analytically but the result is complicated. To relieve the complexity in the free energy expression, therefore, we adopt a limiting case approximation, which is simple and yet accurate enough to explain fairly well the elastic behavior of the deformed film.[29] In this method, the free energy of polymer deformation is expressed as a simple sum of two asymptotes: long-wavelength limit ($t_p q \ll 1$) and short wavelength limit ($t_p q \gg 1$), which leads to the following simplified form:[25]

$$(F_{\text{deform}})_S = \frac{E_p\epsilon^2}{4q^2{t_p}^3} + \frac{1}{6}E_p\epsilon^2 q \tag{6}$$

For the small amplitude ($\epsilon \ll \lambda$) being considered, the external strain U can be approximated by $(\epsilon k/2)^2$.[24] Then, the total energy F_{total} can readily be obtained by summing eqs 3 and 6:

$$F_{\text{total}} = \left(\frac{E_m q^2 {t_m}^3}{12(1-{\nu_m}^2)} + \frac{E_p}{q^4{t_p}^3} + \frac{2E_p}{3q}\right)U \tag{7}$$

The intrinsic wrinkling wavelength can be obtained by minimizing the free energy with respect to the wavenumber and in dimensionless form, it is[17]

$$L = \left(\frac{Y}{1+\sqrt{1+12YH^3}}\right)^{1/3} \text{ where}$$
$$L \equiv \frac{\lambda}{2\pi t_m},\ Y \equiv \frac{1}{2(1-{\nu_m}^2)} \times \frac{E_m}{E_p} \text{ and } H \equiv \frac{t_m}{t_p} \tag{8}$$

As given by eq 8, the characteristic wavelength of the elastic wrinkling is constant, in contrast to the changing wavelength in the viscous wrinkling that is treated later.

One prominent variable yet to be included in eq 8 is the temperature that determines the value of the Young's modulus of the polymer. The bulk modulus of metal can still be used since the metal does not go through a phase change when heated, although the value might be smaller in thin film state due to the porosity or rough interface problems in the thin film

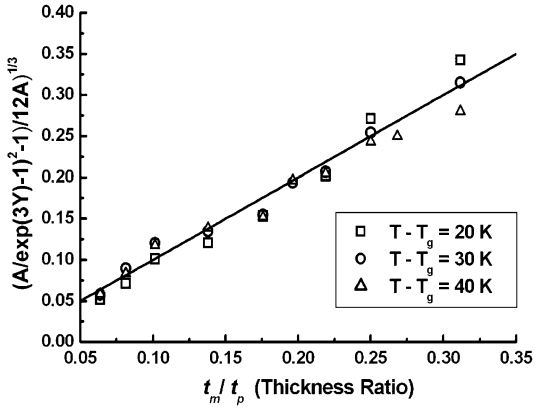

Figure 3. Comparison between theory and experiment for the intrinsic buckling wavelength λ. The theoretical line is that given by eq 8.

state.[30] For viscoelastic polymeric materials, the elastic modulus changes with temperature or time during the heating because of its relaxation characteristics.[31] In general, the temperature dependence of the viscoelastic properties of the polymer can be expressed by the Williams−Landel−Ferry (WLF) equation, which gives $\log(E_p/E_{p,0}) = -\{C_1(T - T_0)/(C_2 + T - T_0)\}$, where $E_{p,0}$ is the E_p at a reference temperature of T_0, which is often taken as T_g of the polymer, and C_1 and C_2 are the experimental constants unique to a given polymeric material. The WLF equation is usually utilized to estimate the dynamic viscosity of the polymer. For polystyrene being used in our system, C_1 and C_2 are 12.7 and 49.8 K respectively according to the literature.[31] Here, we apply the WLF equation for estimating the elastic modulus of the polymer in the temperature range corresponding to the rubbery plateau region, which is slightly above the glass transition temperature. The modulus in this range is known to change much more gradually with temperature than the corresponding viscosity, hence the name rubbery plateau region.[15] Therefore, the values of C_1 and C_2 should be modified to describe the temperature dependency of the modulus in this region. To determine the constants, we prepared various samples with different thickness ratios and carried out wrinkling experiments at 115 and 130 °C ($T - T_0 = 10$ and 25K). The values of C_1 and C_2 that best fit the experimental wavelengths were found to be 3.7 and 2.5 K, respectively.

To test the adequacy of eq 8 in predicting the wavelength with the aid of the constants given above, experiments were carried out at various temperatures in the range where the polymer layer maintains its elastic behavior. For the system being considered, $T_0 =$ 378K (high molecular weight PS, MW = 1340000), $\nu_m = 0.33$, $E_m = 70$ GPa, $E_{p,0} = 3.2$ GPa. Shown in Figure 3 by the solid line is the plot of eq 8 with H ($=t_m/t_p$) as the abscissa, along with the experimental data. It is seen that a good agreement is reached between theory and experiment.

Kinetic Approach for Viscous-Like Polymer Layer If the underlying polymer layer behaves like a viscous medium, the system can be described by a kinetic approach that is based on an instability analysis of continuity equation. At a temperature much higher than T_g, polymer flows readily like molasses and gets into the liquid flow region. For the system in Figure 2, the equation of motion for the lateral flow in the thin film can be written as follows:[32−34]

$$\frac{\partial}{\partial t}h(x,t) = C\frac{\partial^2}{\partial x^2}P[h(x,t)] \tag{9}$$

where $h(x,t)$ is the local film thickness, C is a constant that depends on the shape of the flow profile and the viscosity, and P is the film pressure. For a highly confined system of ours, which is a polymer layer sandwiched between the substrate and the capping layer, the flexural pressure due to the metal bending and the normal stress due to the polymer deformation contribute to the lateral flow of the film, because the polymer is strongly bonded with both the upper and lower layers. If we consider all factors that contribute to the film pressure P, it can be written in the following form:

$$P = D\frac{\partial^4 h}{\partial x^4} - \gamma\frac{\partial^2 h}{\partial x^2} + \frac{A}{6\pi(t_m + t_p)^3} - \sigma_{zz} \tag{10}$$

Here D [$= E_m t_m^3/12(1 - \nu_m^2)$] is the flexural rigidity of the metal,[22] γ is the interfacial tension between the polymer and the metal, A is the effective Hamaker constant describing the van der Waals interactions of the bilayer film,[35] and σ_{zz} is the normal stress due to the deformation in the confined polymer layer. Equation 10 is valid for initial perturbation of the film or $\partial h/\partial x << 1$.

The first term in eq 10 describes the bending pressure of the metal layer and the second term represents the interfacial pressure due to the viscous flow of the confined polymer film. The third term is for the dispersion pressure from the van der Waals interactions in a very thin layered system (less than 100 nm).[36,37] The last term is for the pressure from the normal stress in the deformation of polymer layer,[38,39] which reflects the initial thermal stress above the critical buckling point. It causes the polymer to expand its surface area by changing its shape into a wavy structure to relieve the initial stress from thermal mismatch, which acts as a driving force for generating the buckling wave. While all possible terms are included in eq 10, one or both of the last two terms would drop out depending on experimental conditions such as film thickness and the molecular weight of the polymer. These cases will be discussed in more detail in the next section. Here we include all the terms for a general analysis.

To express σ_{zz} as a function of x and z in eq 10, we resort to eq 5 for the expression of stress−strain relation in deformed elastic layer since $\sigma_{zz} = \mathrm{d}F_{\mathrm{deform}}/\mathrm{d}h$. The normal component contributing to the stress is given by the relation, $\sigma = \sigma_{xx}\sin^2\theta + \sigma_{zz}\cos^2\theta + 2\sigma_{xz}\sin\theta\cos\theta \approx \sigma_{zz}$, since $\tan\theta = \partial h/\partial x \approx 0$. After obtaining the linear strain fields and some algebraic manipulations, we arrive at the expression of σ_{zz} at $z = h_0$ as follows:

$$\sigma_{zz} = \epsilon G\cos(qx)\left[\frac{(1-\nu_p)}{(1-2\nu_p)(1+\nu_p)}\Psi_2'(h_0) + \frac{\nu_p}{(1-2\nu_p)(1+\nu_p)}q\Psi_1(h_0)\right] \tag{11}$$

where E_p has been taken as the relaxation modulus of the polymer, G. Then, we consider the fate of a small fluctuation of the wrinkling wave. Inserting eq 10 into eq 9, and keeping only those terms linear in the

amplitude of the fluctuations and considering small fluctuations of the film in the form of $h(x,t) = h_0 + \epsilon\cos(qx)\exp(t/\tau)$,[32] gives

$$(C\tau)^{-1} = -Dq^6 - \gamma q^4 + \frac{A}{2\pi(t_m + t_p)^4}q^2 + f(qh_0)Gq^3 \quad (12)$$

where $f(qh_0)$ has to do with the normal stress due to the confined polymer that is given by

$$f(qh_0) = \frac{(1-\nu_p)}{(1-2\nu_p)(1+\nu_p)} \times \left[\frac{(qh_0)^2 + \cosh^2(qh_0)}{\cosh(qh_0)\sinh(qh_0) - qh_0} - \frac{\nu_p}{(1-\nu_p)}\frac{(qh_0)^2}{\cosh(qh_0)\sinh(qh_0) - qh_0}\right] \quad (13)$$

and where τ is the growth parameter that determines the film stability. In eq 12, one can find the third term of van der Waals interaction and the fourth term of normal stress of polymer act as destabilizing factors in the buckling (when A is positive) to make a wave to propagate. While the expression for excess free energy is derived from eq 5 for the energetic approach, we should derive an expression for the pressure due to the normal stress of the polymer layer for the kinetic approach taken here. Equation 13 contains highly nonlinear terms with respect to q in the expression $f(qh_0)$, hence it is difficult to solve the stability condition analytically. A simplified form of the pressure due to the normal stress is required as in the free energy approach.

To obtain a simple expression for σ_{zz}, we again turn to the expression for the excess free energy of polymer in eq 5. The expression is a simple linear combination of two asymptotes, one for the long wavelength limit and the other for the short wavelength limit.[25,29] This approximation presents a problem in representing the long wavelength contribution because the contribution disappears in the differentiation for the stability condition. To better represent the rigorous expression of the free energy for the contribution, a correlation method[40] involving two asymptotes and their expansion terms was extended, which gives $F/F_{min} = (0.32qh + 0.48/(qh)^2 + (0.48/(qh)^2)^n)$,[18] where F_{min} is the minimum of F. An n value of 0.7 best fits the rigorous expression.[25] With this relationship, we can arrive at the following expressions for σ_{zz} and $f(qh_0)$ when t_p is equal to h_0: $\sigma_{zz} = \epsilon G\cos(qx) \times (q/2 + {}^3/_4 q^2 t_p{}^3 + 1.87/2q^{1.4}h^{2.4})$, $f(qh_0) = {}^1/_2 + {}^3/_4 q^3 t_p{}^3 + 0.94/q^{2.4}t_p{}^{2.4}$. Then, eq 12 reduces to

$$-(C\tau)^{-1} = \left(\frac{E_m t_m{}^3}{12(1-\nu_m{}^2)}q^6 + \gamma q^4\right) - \left(\frac{A}{2\pi(t_m + t_p)^4}q^2 + \left(\frac{q^3}{2} + \frac{3}{4t_p{}^3} + \frac{0.94q^{0.6}}{t_p{}^{2.4}}\right)G\right) \quad (14)$$

There is still a question as to which G is relevant in eq 14. It is assumed that it is the modulus in the liquid flow region of the confined polymer. Since the instability of the system is determined only by the growth parameter of the wave deflection, the most probable growing mode is one that corresponds to the minimum of τ^{-1} with respect to q. As the relaxation of the polymer progresses, the modulus G in eq 14 changes and so does the wavelength of the wrinkling..

Results and Discussion

We presented theories on the wrinkling for elasticity-governed and viscosity-governed polymer layers. For a given set of wrinkling conditions, the initial state of the polymer could be governed by elasticity or viscosity. Because of the relaxation of polymer with time, however, the polymer behavior eventually becomes governed by viscosity whatever the initial state may be. Therefore, a combination of the two theories applies in general to a given wrinkling. For convenience, the polymer layer governed by elasticity in the initial stage of wrinkling will be referred to as elasticity-governed and the theory under energetic approach in the previous section applies for the initial stage. The term elasticity-retained viscous polymer is used for the case where the normal stress due to the polymer deformation, σ_{zz}, should be retained in eq 10 for the initial stage of wrinkling. The term fully viscous polymer is reserved for the case where σ_{zz} is absent in eq 10.

While the initial state of the polymer is the major factor that determines the wrinkle morphology and its evolution, there are other factors that come into play. These are strain saturation of the metal and pinning of the bilayer to the substrate that can take place. Depending on these factors and the initial state, there are five identifiable wrinkling regimes. Some of these regimes share common characteristics in terms of the change of the wavenumber and that of the strain with time and these five regimes can be grouped into three types. We begin with type I.

Type I: Elastic Wrinkling: Spinodal Wrinkling Regime. Purely elastic wrinkling is typified by the constancy of the wavelength, as shown later with a cross-linked polymer. However, the constancy is maintained only in the initial stage of wrinkling for a viscoelastic polymer. Shown in Figure 4 is the temporal evolution of an elastic wrinkling known as spinodal wrinkling,[17] which will be referred to as "type I wrinkling" , along with Fast Fourier transform (FFT) in the inset of each frame. In this case, a relatively thick film (300−600 nm) of high molecular weight PS (MW = 1340000) was capped with Al film (30−60 nm) and then wrinkled at 140 °C, which is 25 °C higher than T_g. One can observe in the figure two distinct transitions in the evolution of the wrinkling morphology. One is the transition from an islandlike pattern to a labyrinthine pattern as apparent in going from Figure 4a to Figure 4e, while maintaining the wavelength, which can be verified from the constancy of the ring radius in the FFT images. The initial islandlike pattern of very small amplitude grows with time and gets finally saturated to a fully saturated labyrinth pattern in tens of hours of heating at 140 °C. The other transition is marked by the appearance of a second wave, as typified in the FFTs from Figure 1f to Figure 1h, i.e., the emergence of a second ring or a larger wave than in the earlier transition. As time progresses, the larger wave starts exerting itself and becomes dominant over the initial wave.

The growth of waves with time only in the amplitude, which is strain in wrinkling, in the early stage without any change in the wavelength, and the initial emergence of perturbational islandlike fluctuation are similar to those found in the early stage of spinodal decomposi-

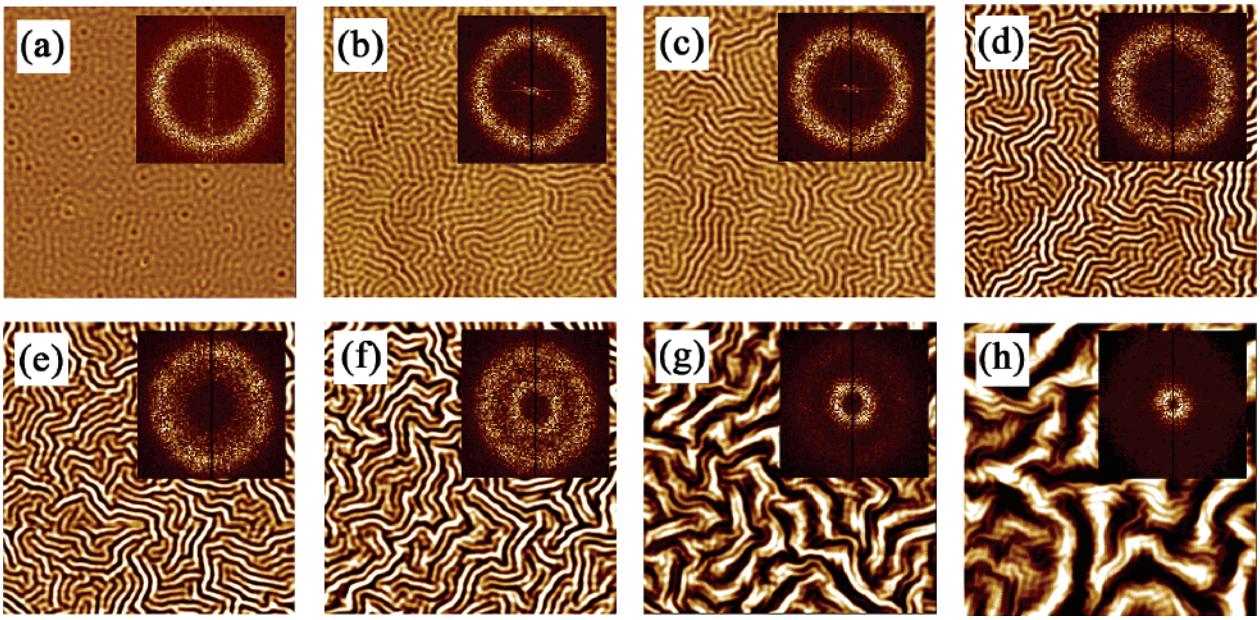

Figure 4. AFM images (80 μm × 80 μm) of temporal evolution of wrinkled surfaces that result with a 40 nm thick metal layer and a 350 nm thick high molecular weight polymer layer at 140 °C. Resulting intrinsic wrinkling wavelength is 2.45 μm. Insets show the fast Fourier transform (FFT) images for given patterns. A ring in the FFT indicates that an isotropic single length-scale pattern is dominant. Key: (a) pattern after 3 min; (b) pattern after 20 min; (c) pattern after 3 h; (d) pattern after 12 h; (e) pattern after 36 h; (f) pattern after 72 h; (g) pattern after 100 h; (h) final pattern after 170 h.

tion.[41,42] The constant wavelength in the early stage can be determined by the elastic wrinkling theory, which is based on the free energy approach. On the other hand, the emergence of a second peak means that a new wavelength parameter intervenes and interacts with the initial wavelength. An interesting fact in the late stage is that the strain of the metal layer remains constant even with increasing wavelength. This type of behavior in strain−time relationship is the same as in creep and relaxation loading for the mechanical response of polymer.[43] No increase in strain in late stage suggests that the stress relaxation lies in the polymer layer.

For an analysis of the late stage, one can utilize the kinetic approach, in which the relaxation of polymer is represented by the value of the relaxation modulus. This relaxation process can be described quantitatively with the calculation steps presented in the following section for viscous wrinkling. The wave growth in the late stage is restricted by the limited film thickness. Although the wave can grow continuously, the wavy pattern becomes "pinned" after a long period of heating as shown in Figure 4h because of its finite thickness in the polymer layer. This pinning hinders the amplification of waves. A sectional micrograph by scanning electron microscopy was also used to verify the fact that the valleys of the wrinkles indeed reached the substrate surface, which confirms the pinning behavior.

To investigate purely elastic wrinkling, we hardened the underlying polymer layer by exposure to ultraviolet light.[44,45] For the cross-linking, an ultraviolet ray (wavelength = 254 nm) was irradiated on the PS surface for 40 min since excessive irradiation can break the polymer chain. No wrinkling took place at 140 °C, which was used for non-cross-linked PS, and the temperature had to be raised to 170 °C for the wrinkling. This fact is an indication that the cross-linking preserves the elastic behavior of the polymer to a much higher temperature than otherwise, because the relaxation motion of entangled chain is restricted by the cross-linked sites between chain molecules.[15]

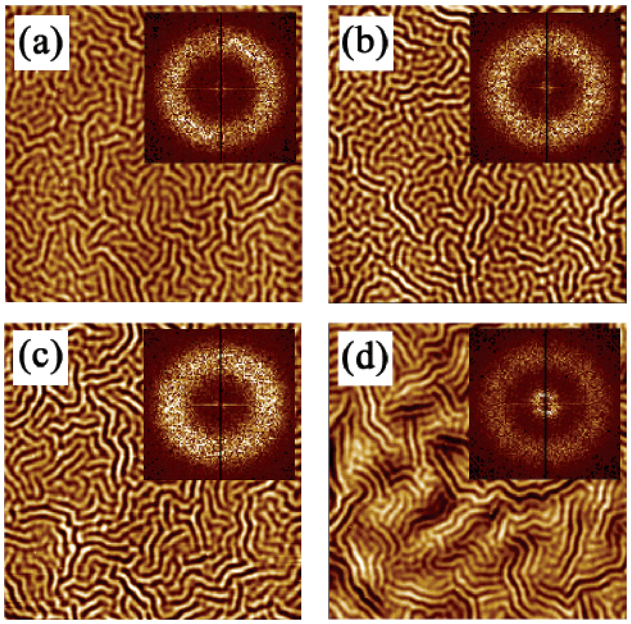

Figure 5. AFM images (80 mm × 80 mm) of temporal evolution of wrinkled surfaces that result with a 35 nm thick metal layer and a 250 nm thick and lightly cross-linked high molecular weight polymer layer at 170 °C. Key: (a) pattern after 20 min; (b) pattern after 3 h; (c) pattern after 48 h; (d) final pattern after 100 h.

Figure 5 shows the wrinkling behavior of the lightly cross-linked polymer. Two transitions that correspond to the constant wavelength growth in the early stage and the late emergence of a larger wave as in the spinodal wrinkling are also observed. However, there exists a distinct difference. Although the second larger wave having a small amplitude can be seen in the cross-linked case, the viscous response of the underlying polymer was highly suppressed, which can be verified in Figure 5d for the final state of the wrinkling. If the cross-linking density in the polymer is increased, there-

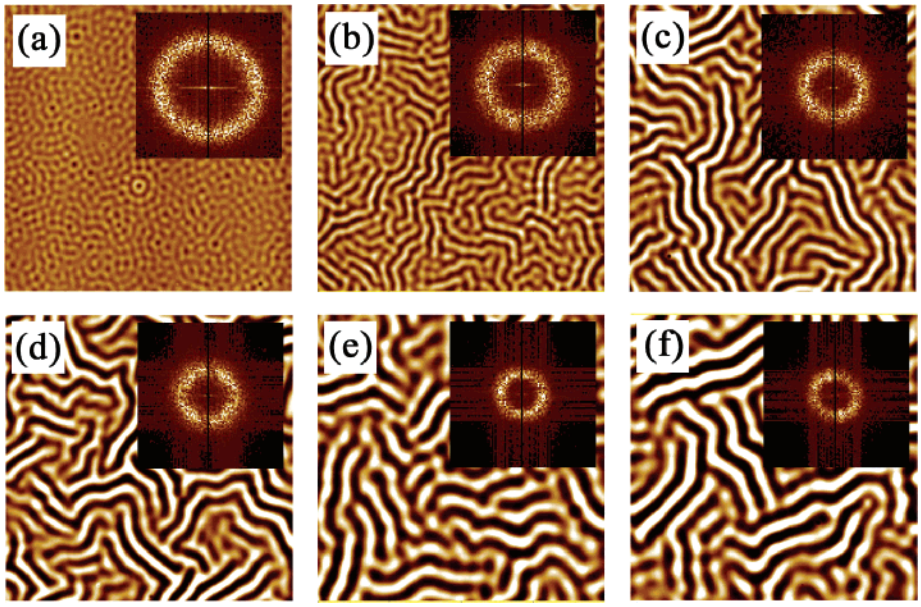

Figure 6. AFM images (80 μm × 80 μm) of temporal evolution of wrinkled surfaces that result with a 40 nm thick metal layer and a 350 nm thick high molecular weight polymer layer at 160 °C. Key: (a) pattern after 2 min; (b) pattern after 3 min; (c) pattern after 10 min; (d) pattern after 1 h; (e) pattern after 6 h; (f) final pattern after 24 h.

fore, one could expect the fully elastic wrinkling in which the wavelength remains constant.

The type I wrinkling is typified by the elastic wrinkling that takes place in the early stage. Accordingly, the elastic behavior of polymer plays an important role in the bilayer wrinkling and the bilayer system can be analyzed on the basis of the energetic approach in which the polymer is treated as an elastic rubber. The resulting wrinkle wavelength can be obtained by minimizing the total free energy. When relaxation takes place in the polymer layer with time, the wrinkle grows with time, which is a characteristic of viscous wrinkling. The wrinkling that is determined mainly by the elasticity in the early stage and then by the viscosity in the late stage, subject to strain saturation and bilayer pinning, is spinodal wrinkling. The final morphology arrived in this spinodal wrinkling is a mountainous structure that is shown in Figure 4h.

Type II: Viscous Wrinkling (Strain Saturation). There are three regimes in type II wrinkling, but they share common characteristics in terms of wavenumber and strain behavior. In this type II wrinkling, the wavelength keeps increasing with time, typical of the viscous wrinkling, but it is restrained by the strain saturation of the metal. Depending on whether the pinning occurs in the early stage of wrinkling or the late stage, there results "constrained evolutionary" or "evolutionary wrinkling" . Under certain wrinkling conditions, the wrinkling takes place instantaneously without any incubation period and thus this regime may be called "instantaneous wrinkling" as opposed to the evolutionary wrinkling. In this third regime of type II wrinkling, the pinning takes place immediately after wrinkling.

(a) Evolutionary Wrinkling Regime. Shown in Figure 6 is the typical temporal evolution of the evolutionary wrinkling. The wrinkling conditions are similar to those in Figure 4, the only difference being the processing temperature. As given in the figure, 160 °C was used for the wrinkling, which is 55 °C higher than the T_g of PS and 20 °C higher than that in the spinodal wrinkling (Figure 4). In general, a polymer undergoes two stages of thermomechanical transition during the heating process. One is the transition into rubbery state at slightly above the glass transition temperature, which corresponds to the rubbery plateau region where the modulus decreases gradually. The other is the transition into viscous flow state at much higher temperature. For PS, the transition to the viscous flow state occurs around 160 °C for the high molecular weight PS being considered. Hence, this temperature will be referred to as "flow temperature". Industrial processing of PS is usually performed above this temperature. Although there is only a 20 °C difference in the heating temperature between Figure 4 and Figure 6, the behavior of the underlying PS layer is completely different at 160 °C. While the polymer in Figure 4 maintains its elastic behavior during the wrinkling, the polymer in Figure 6 behaves like a viscous liquid.

There are two distinct features in the evolution of the wrinkling morphology. One is the wave growth with time in the early stage as apparent in going from Figure 6a to Figure 6e. The other is the constancy of the wavelength in the late stage as shown from Figure 6e to Figure 6f, which is similar to the pinning behavior in the late stage of spinodal wrinkling.[17] To analyze this viscous wrinkling, we turn to eqs 9 and 14 in the theory section. Although there are several terms in eq 14, only two terms turn out to dominate the system under consideration. One is the bending force from the metal, and the other is the normal stress from the deformation of the confined polymer. The bending force is larger than the interfacial tension by an order of magnitude in the first bracket of eq 14 and the normal stress overwhelms the dispersion force by 4 orders of magnitude in the second bracket.[46] On the basis of eq 14 with the aid of physical parameters, the values of G can be calculated that yield the experimental wavelength for the initial wave emergence (the fastest growing wave, 4.03 μm (Figure 6a) and that for the saturation wave (6.21 μm (Figure 6, parts e and f). The modulus values thus calculated are 2 MPa and 100 kPa, respectively. The modulus of 2 MPa for the initial wrinkling indicates that

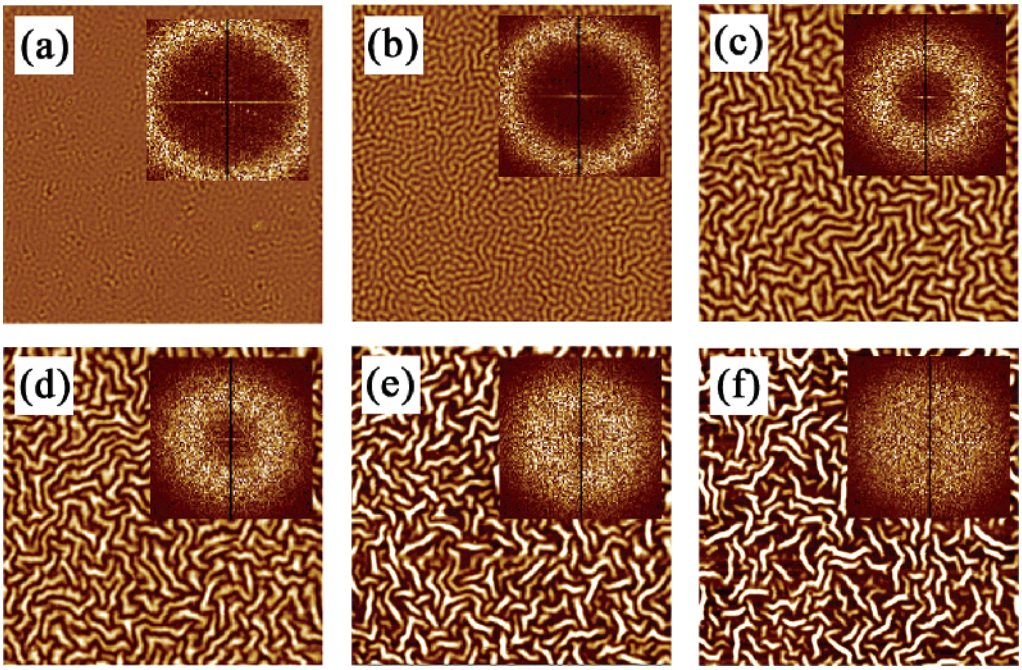

Figure 7. AFM images (80 μm × 80 μm) of temporal evolution of wrinkled surfaces that result with a 30 nm thick metal layer and a 46 nm thick high molecular weight polymer layer at 180 °C. Key: (a) pattern after 30 min; (b) pattern after 1 h; (c) pattern after 1.5 h; (d) pattern after 2 h; (e) pattern after 6 h; (f) final pattern after 24 h.

the wrinkling process is initiated by the rapid decrease of the modulus from the hard glassy to soft rubbery state. Although the transition can also be found in the elastic wrinkling, the modulus decreases rapidly with time above the flow temperature, where the viscous wrinkling dominates the system. The decrease in modulus to about 100 kPa is an indication that the relaxation toward a liquid state of the polymer proceeds continuously with time, which is expected from the relaxation behavior of the polymer.

The other feature of constant wavelength can be interpreted in the same way as with the pinning behavior in spinodal wrinkling in Figure 4. While the restricted strain increase in the metal layer leads to the transition from the early to late stage in spinodal wrinkling, the strain keeps increasing in the viscous wrinkling without any restriction with the wavelength. When the maximum strain at the wave saturation is reached, then the wrinkles stop growing due to the pinning as shown in Figure 6f. After the pinning, no more change in wrinkled morphology is observed. The final morphology reached in the evolutionary wrinkling is a labyrinth structure. The common feature in the elasticity-retained viscous wrinkling is that the wrinkles evolve continuously to a final morphology as opposed to purely viscous wrinkling in which the wrinkles eventually disappears in the absence of the pinning. The evolution in this wrinkling regime is constrained only by the pinning in the late stage.

(b) Constrained Evolutionary Wrinkling Regime. In this elasticity-retained viscous wrinkling, pinning occurs in the early stage of wrinkling. The early pattern continues evolving even after the pinning because the metal strain is not saturated, which enables the continuous evolution even after the pinning.

Shown in Figure 7 is the typical temporal pattern evolution in this constrained evolutionary wrinkling. A high molecular weight PS was used for the wrinkling and the PS film was very thin (less than 100 nm). Wrinkling was carried out at 180 °C, which is 75K higher than T_g.[18] The reason for such a high temperature is that the critical compressive stress increases rapidly for the very thin polymer layer. Consequently, a very high temperature is needed to overcome the critical stress and induce the wrinkling, As was done in the previous section, G values of 500 and 30 kPa can be calculated from the experimental wavelength for the initial wave emergence (the fastest growing wave, 1.73 μm, Figure 7a) and that for the saturation wave (3.52 μm, Figure 7d), respectively. The modulus of 500 kPa means that the liquid flow state (less than MPa) of the polymer can initiate the thin film wrinkling. In addition, the change of modulus from 500 to 30 kPa is an indication that the relaxation toward a liquid state of the polymer proceeds with time, which is similar to the thick film case in Figure 6. A larger decrease in the final modulus, compared with that in the thick film case, could possibly come from the wrinkling under a much higher temperature (180 °C).

An immediate observation from Figure 7 is that the wavelength increases with time (from Figure 7a to Figure 7d), although the wavelength reaches a plateau after a few hours, which is similar to the behavior of the evolutionary wrinkling shown in Figure 6. A distinct difference, however, can be found in that there is a transition from the continuous wavy pattern to a discrete wormlike pattern (Figures 7e and 7f).[18] The sectional AFM analysis of the samples of Figure 7d and Figure 7f shows that in both cases, the patterns are "pinned" because the valleys of the wrinkles reached the substrate surface. An intriguing aspect of the transition, unique to this very thin film, is that the wavy pattern still evolves to the wormlike pattern even after the pinning, in contrast to the spinodal wrinkling (Figure 4) and the evolutionary wrinkling (Figure 6) in which no pattern evolution is observed after the pinning. The main difference lies in the fact that the pinning in other cases occurs after the strain saturation and thus the metal can no longer be stretched; for the very thin film being considered, the pinning occurs before the strain

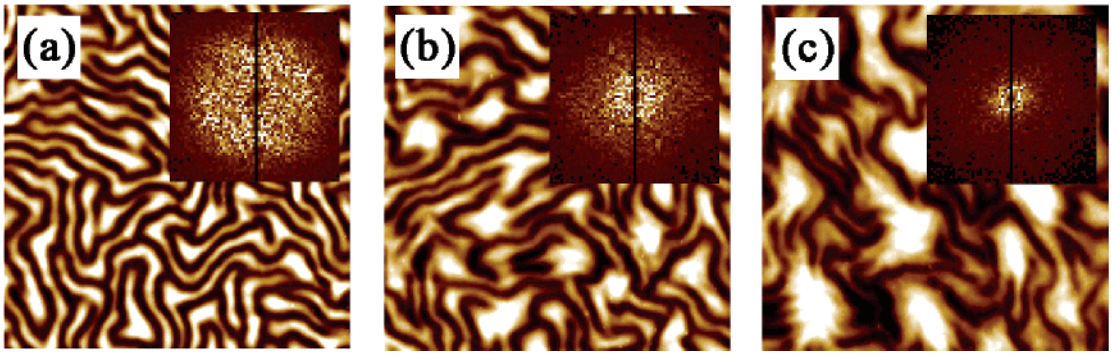

Figure 8. AFM images (80 μm × 80 μm) of temporal evolution of wrinkled surfaces that result with a 35 nm thick metal layer and a 60 nm thick low molecular weight polymer layer at 160 °C. Key: (a) pattern after 2 min; (b) pattern after 5 min; (c) final pattern after 24 h.

saturation. Therefore, the metal can still expand even after the pinning. A fact relevant to the morphology transition is that the wavelength of wrinkles remains constant even after the pinning but with an accompanying increase in the amplitude and the roughness. The only way for the amplitude to increase after the pinning with a constant wavelength is through annihilation of the waves of less dominant modes, which leads to the final morphology of a wormlike island structure. It is a pinned flat surface with islands.

In the two wrinkling regimes considered so far, the viscous state dominates the system due to the annealing at a high temperature that is much above the "flow temperature" of the polymer. However, the elastic behavior of the polymer as represented by the normal stress within the confined state still plays an important role in the wrinkling process. This elastic behavior in the viscous state originates from the strong confinement between the substrate and the capping layer. For an analysis of this elasticity-retained viscous wrinkling, eq 14 was used, in which the elastic relaxation of polymer acts as a counterforce term against the metal bending term. The relaxation in the polymer layer results in an increase in the wavelength as the relaxation modulus decreases with time.

(c) Instantaneous Wrinkling Regime. Wrinkling of very thin films (<100 nm) of low molecular weight polymer leads to instantaneous formation of an island structure without incubation period. The fully viscous nature of the low molecular weight polymer at the high temperature needed for the wrinkling is responsible for the instantaneous pinning and saturation that take place in the wrinkling.

Figure 8 is a typical example that results when a very thin polymer layer of low molecular weight is wrinkled at a very high temperature (about more than 70−80 K higher than T_g). In this case, an island structure results eventually, which is similar to the final stage of Figure 7. The abruptly generated stress due to the high temperature heating cannot be fully dissipated into the viscous polymer layer because of the thickness restriction. Once the islands form as in Figure 8c, a viscous polymer is confined within the isolated islands capped with the metal layer, in which the polymer cannot make any motion to relieve the excess stress from the high temperature heating, resulting in the pinning.

Type III: Viscous Wrinkling (Biphasic Strain). Unconstrained Wrinkling Regime. This regime is fully governed by the viscous nature of the polymer that is unhindered either from the pinning or the strain saturation, hence the name "unconstrained wrinkling". Relatively thick films of low molecular weight polymer are involved in this unconstrained wrinkling.

Shown in Figure 9 is the typical temporal evolution of the unconstrained wrinkling. An important factor in "type III wrinkling" is that a low molecular weight PS (MW = 8500) is used for the wrinkling. This value of molecular weight is smaller than its entanglement molecular weight (for PS = 18 000) such that the molecular motion of the polymer above the T_g shows a fully viscous behavior. Any experimental and analysis should take account of the fact that the T_g is lower than that of high molecular polymer. In fact, the glass transition temperature decreases to about 80 °C. In Figure 9, as expected, a morphological transition for viscous wrinkling is observed in the early stage of wrinkling, which is typified in Figure 9a through Figure 9d. In a short period of about 30 min, waves emerge and grow to larger ones with increasing surface roughness (strain in the metal layer).[47] Interestingly, however, the wave intensity decreases after some time and the surface gets nearly flattened eventually as shown in Figure 9f. The strain in the metal layer reaches the maximum of 0.005 (1% increase in area) in Figure 9d and then decreases with time to 0.00008 (0.02% increase in area) in Figure 9f. Although there remain some traces of the wrinkles due to the bending in the metal layer, the surface can practically be treated as a nearly flat state (height variation is less than 10 nm). The traces of wrinkles of the flat surface are similar to those found on the flattened surface of once wrinkled paper.

The behavior in which the strain increases with time initially but then decreases later to almost no strain is a characteristic unique to the unconstrained wrinkling. What happens physically is that the metal stretched by the polymer (maximum strain of 0.005 or 1% increase in area) reverts and retracts back to the original state of the metal (strain of 0.00008 or 0.02% in area), once the stress gets relieved in the viscous polymer layer. Further study would be required for a quantitative explanation of the behavior as discussed shortly.

As the elastic nature of the polymer is completely removed in this low molecular weight case, the wrinkling phenomenon can be described by the interaction between the metal bending and the interfacial tension. Therefore, the instability condition of eq 12 for this relatively thick films reduces to

$$(C\tau)^{-1} = -\frac{E_m {t_m}^3}{12(1-{\nu_m}^2)} q^6 - \gamma q^4 \qquad (15)$$

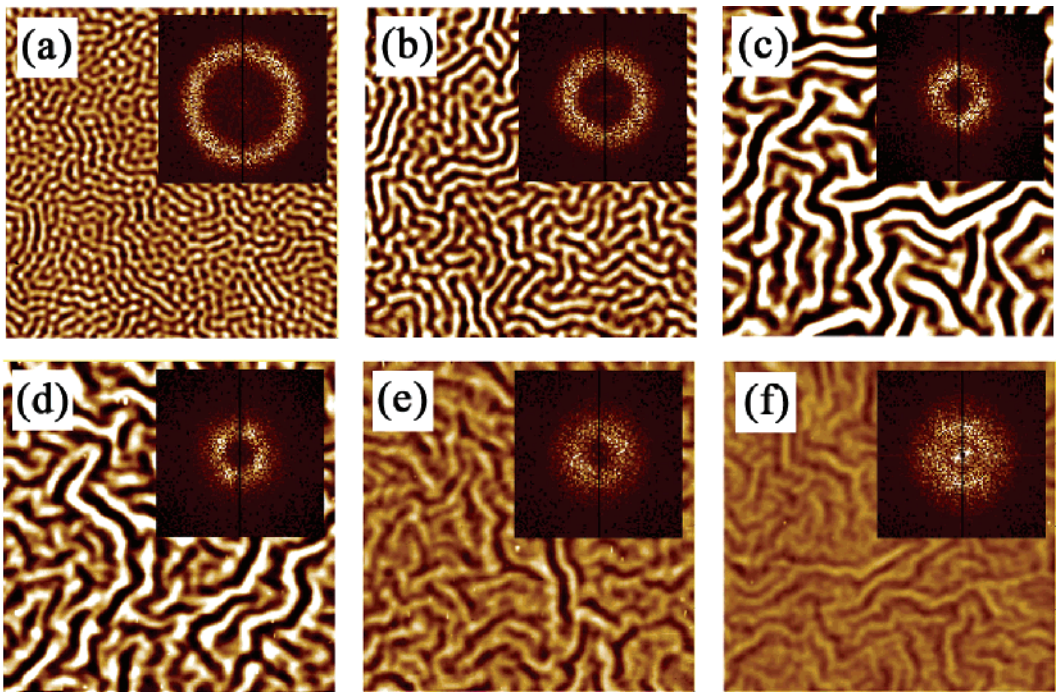

Figure 9. AFM images (80 μm × 80 μm) of temporal evolution of wrinkled surfaces that result with a 40 nm thick metal layer and a 400 nm thick low molecular weight polymer (MW = 8500) layer at 120 °C. Key: (a) pattern after 6 min; (b) pattern after 15 min; (c) pattern after 25 min; (d) pattern after 30 min; (e) pattern after 1 h; (f) final pattern after 36 h.

The two terms in eq 15 are not competitive with each other. Instead, both act as stabilizing factors, which yields a zero wavenumber as the fastest growing wave. Therefore, an infinite sized wrinkle is the dominant one. The emergence of an infinite wavelength wrinkle can be verified indirectly from the FFT image in Figure 9f in which a high-intensity bright spot is located in the center part of the Fourier space. The corresponding wavelength of the peak is 27 μm and it is about 60 times larger than the bilayer thickness (440 nm), which shows the system's attempt toward an infinite-size wrinkle.

However, the biphasic nature of the strain still remains unexplained quantitatively, in particular, the decrease in the intensity of the waves in the late stage and the final flatness of the surface. The dynamic approach used here for the viscous wrinkling on the basis of a continuity equation is not effective for the estimation of the intensity (amplitude) of the wave. In the approach, the amplitude of the wave is assumed to be much smaller than the wavelength of the wave.[32−34] Once the wavelength is determined from the stability condition, the amplitude is treated to be proportional to the resulting wavelength. According to this assumption, an infinite wavelength wrinkle should generate an infinite amplitude, which is impossible to take place under the typical experimental conditions. For the reason the amplitude decreases, the linear stability approach could be taken that is based on a stress analysis for the bilayer in which the original in-plane stress is taken into consideration.[12−14] This numerical approach could describe the amplitude change and the saturation process during the wrinkling. While it is suitable for the explanation of the early stage of the wrinkling, however, it is still difficult to estimate the state of wrinkles after long time evolution. Recently, an approximate nonlinear method is utilized to estimate the post-buckling kinetics in wrinkling.[48] In that approach, the longest wavelength of wrinkle (infinite wavelength) is expected to be the only dominant wave eventually. The amplitude should decay by the releasing of the compressive stress and the bending energy of the bilayer film, resulting in a completely flat film. A quantitative explanation by this approximate nonlinear method needs to be modified to a more complicated form for it to be applied to our system, which is beyond the scope of this article.

There have been theoretical results[48,49] showing that the viscous wrinkling would eventually leads to a flat surface. The result shown here is the first experimental evidence that the wrinkled surface eventually becomes flat.

Conclusions

We have presented five wrinkling regimes that are defined primarily by the thermomechanical behavior of the polymer and by strain saturation and bilayer pinning, and grouped them into three types of wrinkling. To help understand the three types of wrinkling, a simplified morphological diagram is given in Figure 10 in terms of film thickness and processing temperature with the molecular weight of polymer as a parameter. For the high molecular weight case, shown in Figure 10a, a retained elastic response of polymer even above the glass transition temperature provides the elastic contribution during the wrinkling, which leads to various wrinkling morphologies. When the film thickness is very thin (less than 100 nm), the critical compressive stress for wrinkling is very high such that a high temperature annealing is needed to initiate the wrinkling. When the temperature is relatively low, the accumulated thermal stress does not add up to the critical value and no wrinkling is observed on the surface. If the temperature is higher than the flow temperature of the polymer, however, an elasticity-retained viscous wrinkling (type II-b) takes place, but the wrinkling is obstructed by the thickness restriction. In this constrained evolutionary wrinkling, the final morphology is a wormlike island structure.

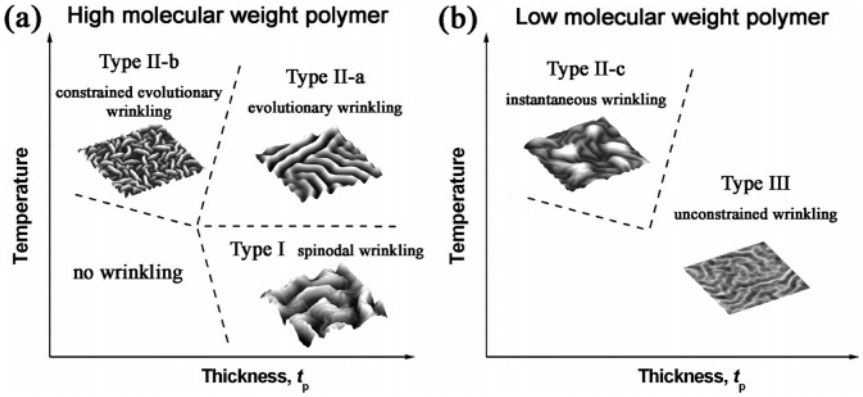

Figure 10. Simplified morphological diagrams for the bilayer wrinkling in terms of thickness and annealing temperature. Typical evolutional characteristics are determined by elastic wrinkling (type I) or viscous wrinkling (type II and III). Insets are three-dimensional AFM images for the final morphology of each wrinkling regime. (a) High molecular weight polymer layer. (b) Low molecular weight polymer layer.

On the other hand, when the film thickness is relatively thick (more than a few hundred nm), the critical stress is sufficiently lowered in such a way that the wrinkling can be initiated by a small amount of thermal stress. If the temperature is slightly above the T_g of polymer, the underlying polymer is in the rubbery plateau region in terms of the modulus and behaves elastically. The elastic approach that is based on free energy minimization can be applied to this case. Because of the similarity with the spinodal decomposition, it can be called spinodal wrinkling (type I) and the final morphology is a mountainous structure. When the temperature is relatively high, however, the underlying polymer layer is in the liquid flow region so that the elasticity-retained viscous wrinkling (type II-a) without the thickness restriction dominates the system. In this evolutionary wrinkling regime, the final morphology is a labyrinth structure.

Low molecular weight polymer makes the system much simpler than the high molecular weight polymer. In this case, the underlying polymer layer shows fully viscous behavior so that the system tends to favor lower frequency mode and finally approaches an infinite wavelength wrinkle. The stress dissipation into the underlying viscous layer makes the surface eventually flat (type III). When the film is too thin, however, the generated stress runs into film thickness restriction before the saturation mode, which results in an island structure (type II-c). In this instantaneous wrinkling regime, there is no incubation period and the wrinkles form instantaneously at the wrinkling temperature.

The five wrinkling regimes can be grouped into three types according to the common characteristics of these regimes. These types can first be characterized in terms of the evolution of wavenumber with time, shown in Figure 11. For the type I (spinodal wrinkling), two distinct constant wavenumber regions exist that correspond to the elastic growth in the early stage and the pinning in the strain saturation stage, respectively. Thus, two transition points exist during the evolution ($t_{I,1}$ and $t_{I,2}$). For the elasticity-retained viscous wrinkling and instantaneous wrinkling of type II, the initial wrinkle wavenumber continuously decreases with time due to the modulus relaxation in the polymer or instantaneous growth followed by pinning and only one constant wavenumber region exists that is caused by pinning (t_{II}). For the type III wrinkling, however, initial viscous wrinkling gradually weakens and the waves

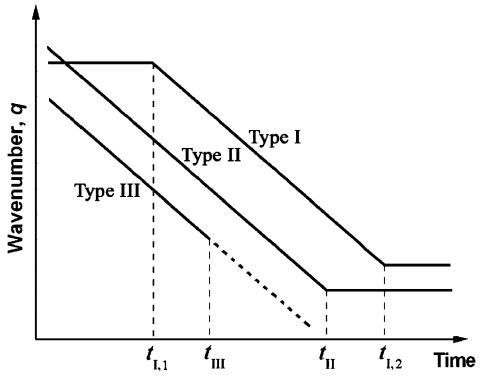

Figure 11. Dominant wavenumber-time relation for three types of wrinkling. Lines are drawn to show the general characteristics. Actual values of time or wavenumber and slopes of the lines depend on experimental conditions. Times ($t_{I,1}$, $t_{I,2}$, t_{II}, t_{III}) indicate the transition points in wave growth.

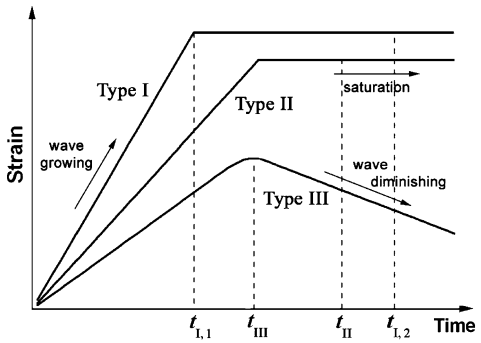

Figure 12. Surface strain−time relation for three types of wrinkling. Lines are drawn for the general characteristics. Actual values of time or strain and slopes of the lines depend on experimental conditions.

diminish in size because of the stress dissipation, for which a dotted line is used in Figure 11(t_{III}).

Another characteristic that is representative of these types is the surface strain evolution in the metal layer with time, shown in Figure 12. To obtain the strain in the metal layer, an indirect method of measuring the average surface area was used. This measurement can provide one with the amount of one-dimensional extension in the metal layer, which can be converted to the value of strain. Interestingly, the strain behavior is similar for both types I and II, which shows a continuous increase with time followed by a constant strain region. The reason for the similarity despite the difference in

the driving force for the wrinkling, i.e., elastic or viscous wrinkling, is that the elastic contribution plays an important role in both types, although the fully viscous type II-c is governed by instantaneous wrinkling followed by pinning. In the early stage of wrinkling, the wave growth in amplitude or wavelength increases the strain on the surface that is driven by the accumulated stress in the bilayer. The strain eventually reaches the maximum and saturates. For the low molecular weight polymer in type III wrinkling, a different strain evolution takes place as shown in Figure 12. In this case, the wrinkles grow with the corresponding increase in the strain. In due time, however, a fully viscous layer due to the molecular weight lower than the entanglement molecular weight makes it possible to dissipate the stress via a long time vibration of bilayer, which leads to the perfectly flat surface. Since the surface is restored to its initial state by flattening, the strain also decreases, eventually approaching zero strain. This biphasic behavior of strain is characteristic of the type III.

It should be noted that no scale was used in Figure 10 because the values of the film thickness and the temperature depend on the pair of polymer and metal used. However, the film thickness marking different regimes is about 300 nm for high molecular weight polymer and around 100 nm for low molecular weight polymer. No scale was used in Figures 11 and 12 for the same reason since it is sufficient to show the general characteristics for the various types of wrinkling.

In summary, we have identified five wrinkling regimes in the wrinkling of a bilayer film of polymer and metal, and grouped them into three types according to the characteristics of the wrinkle growth and morphological features. The thermomechanical behavior of the polymer layer is mainly responsible for the fate of the wrinkles, which is determined by temperature for a given polymer. Because of the constraint arising from the film thickness and its effect on the critical stress needed for the wrinkling, the temperature and the film thickness have been used to construct morphological diagrams for the wrinkling.

In type I wrinkling, the elastic behavior of high molecular weight polymer is still retained in the moderate temperature range so that the wrinkles are generated in such a way to minimize the total free energy of the system. When the temperature is raised above the flow temperature of the polymer, however, the polymer changes into viscous state and the wrinkling wavelength is determined by the stability equation of the dynamic approach, which leads to type II wrinkling. If the molecular weight of the polymer is low enough to lose its elastic characteristic, type III wrinkling governs the system and the wrinkles vanish after some period of fluctuation on the surface.

We expect that this study would be helpful for the understanding of the thermomechanical behavior of the thin polymer film that is placed in the confined state, which is quite different from that in the bulk state and has hardly been dealt with. The results could also provide a solution to increasing needs of a tunability for the stress control in multiplayer in microelectonics and organic devices.

References and Notes

(1) Timoshenko, S. P.; Gere, G. M. *Theory of Elastic Stability*; McGraw-Hill: New York, 1961.
(2) Hutchinson, J. W.; Suo, Z. *Adv. Appl. Mech.* **1992**, *29*, 63.
(3) Suo, Z. *J. Mech. Phys. Solids* **1995**, *43*, 829.
(4) Iacopi, F.; Brongersma, S. H.; Maex, K. *Appl. Phys. Lett.* **2003**, *82*, 1380.
(5) Serrano, J. R.; Cahill, D. G. *J. Appl. Phys.* **2002**, *92*, 7606.
(6) Bowden, N.; Brittain, S.; Evans, A. G.; Hutchinson, J. W.; Whitesides, G. M. *Nature (London)* **1998**, *393*, 146.
(7) Huck, W. T. S.; Bowden, N.; Onck, P.; Pardoen, T.; Hutchinson, J. W.; Whitesides, G. M. *Langmuir* **2000**, *16*, 3497.
(8) Bowden, N.; Huck, W. T. S.; Paul, K. E.; Whitesides, G. M. *Appl. Phys. Lett.* **1999**, *75*, 2557.
(9) Yoo, P. J.; Park, S. Y.; Suh, K. Y.; Lee, H. H. *Adv. Mater.* **2002**, *14*, 1383.
(10) Yoo, P. J.; Park, S. Y.; Kwon, S. J.; Suh, K. Y.; Lee, H. H. *Appl. Phys. Lett.* **2003**, *83*, 4444.
(11) Kwon, S. J.; Yoo, P. J.; Lee, H. H. *Appl. Phys. Lett.* **2004**, *84*, 4487.
(12) Sridhar, N.; Srolovitz, D. J.; Suo, Z. *Appl. Phys. Lett.* **2001**, *78*, 2482.
(13) Huang, R.; Suo, Z. *J. Appl. Phys.* **2002**, *91*, 1135.
(14) Huang, R.; Suo, Z. *Int. J. Solids Struct.* **2002**, *39*, 1791.
(15) Sperling, L. H. *Physical Polymer Science*; John Wiley & Sons: New York, 2001.
(16) Mark, J. E. *Polymer Data Handbook*; Oxford University Press: New York, 1999.
(17) Yoo, P. J.; Lee, H. H. *Phys. Rev. Lett.* **2003**, *91*, 154502.
(18) Yoo, P. J.; Suh, K. Y.; Kang, H.; Lee, H. H. *Phys. Rev. Lett.* **2004**, *93*, 034301.
(19) Allen, H. G. *Analysis and Design of Structural Sandwich Panels*; Pergamon: New York, 1969.
(20) Golubovic, L.; Moldovan, D.; Peredera, A. *Phys. Rev. Lett.* **1998**, *81*, 3387.
(21) Cerda, E.; Mahadevan, L. *Phys. Rev. Lett.* **2003**, *90*, 074302.
(22) Landau, L. D.; Lifshitz, E. M. *Theory of Elasticity*; Pergamon: Oxford, England, 1970.
(23) Audoly, B. *Phys. Rev. Lett.* **1999**, *83*, 4124.
(24) Groenwold, J. *Physica A* **2001**, *298*, 32.
(25) Fredrickson, G. H.; Ajdari, A.; Leibler, L.; Carton, J. *Macromolecules* **1992**, *25*, 2882.
(26) Xi, H. W.; Milner, S. T. *Macromolecules* **1996**, *29*, 4772.
(27) Wallace, W. E.; van Zanten, J. H.; Wu, W. L. *Phys. Rev. E* **1995**, *52*, R3329.
(28) van Zanten, J. H.; Wallace, W. E.; Wu, W. L. *Phys. Rev. E* **1996**, *53*, R2053.
(29) Wang, J.; Tolan, M.; Seeck, O. H.; Sinha, S. K.; Bahr, O.; Rafailovich, M. H.; Sokolov, J. *Phys. Rev. Lett.* **1999**, *83*, 564.
(30) Zhao, J. H.; Du, Y.; Morgen, M.; Ho, P. S. *J. Appl. Phys.* **2000**, *87*, 1575.
(31) Ferry, J. D. *Viscoelastic Properties of Polymers*; John Wiley & Sons: New York, 1980.
(32) Oron, A.; Davis, S. H.; Bankoff, S. G. *Rev. Mod. Phys.* **1997**, *69*, 931.
(33) Herminghaus, S. *Phys. Rev. Lett.* **1999**, *83*, 2359.
(34) Suh, K. Y.; Lee, H. H. Phys. *Phys. Rev. Lett.* **2001**, *87*, 135502.
(35) Israelachvili, J. N. *Intermolecular and Surface Forces*; Academic Press: New York, 1992.
(36) David, M. O.; Reiter, G.; Sitthai, T.; Schultz, J. *Langmuir* **1998**, *14*, 5667.
(37) Yoo, P. J.; Suh, K. Y.; Lee, H. H. Lee, *Macromolecules* **2002**, *35*, 3205.
(38) Safran, S. A.; Klein, J. *J. Phys. II* **1993**, *3*, 749.
(39) Palasantzas, G.; De Hosson, J. T. M. *J. Appl. Phys.* **2003**, *93*, 893.
(40) Churchill, S. W. *The Interpretation and Use of Rate Data: The Rate Concept*; MaGraw-Hill: New York, 1974; p 290.
(41) Cahn, J. W. *Trans. Metall. Soc. AIME* **1968**, *242*, 166.
(42) Bates, F. S.; Wiltzius, P. *J. Chem. Phys.* **1989**, *91*, 3258.
(43) Wineman, A. S.; Rajagopal, K. R. *Mechanical Response of Polymers*; Cambridge: New York, 2000.
(44) Liu, Y.; Russell, T. P.; Samant, M. G.; Stohr, J.; Brown, H. R.; Cossy-Favre, A.; Diaz, J. *Macromolecules* **1997**, *30*, 7768.
(45) Chou, K. F.; Lee, S.; Harmon, J. P. *Macromolecules* **2003**, *36*, 5683.
(46) Dalnoki-Veress, K.; Nickel, B. G.; Dutcher, J. R. *Phys. Rev. Lett.* **1999**, *82*, 1486.
(47) Moldovan, D.; Golubovic, L. *Phys. Rev. Lett.* **1999**, *82*, 2884.
(48) Sridhar, N.; Srolovitz, D. J.; Cox, B. N. *Acta Mater.* **2002**, *50*, 2547.
(49) Liang, J.; Huang, R.; Yin, H.; Sturm, J. C.; Hobart, K. D.; Suo, Z. *Acta Mater.* **2002**, *50*, 2933.

MA048452+